ISSN: 0369-8963

Ann Inspired Mineral Oil Pollution Detection In Marine Environment Using Synthetic Aperture Radar

S. ARIVAZHAGAN[1].M.MARY ROSALINE TAMIL SELVI[1*], T.V. KARTHIKESWARAN[1], V. KUBERAN[1], S. HARIHARAN[1]

[1]Mepco Schlenk Engineering College,Sivakasi, Tamilnadu, India.

**Corresponding author: maryrosaline@mepcoeng.ac.in*

Abstract – *Mineral Oil spills are the predominant disasters that threaten the ocean ecosystem and affect the water lives. To anticipate, prevent, and clean up oil contamination, it is necessary to detect and monitor oil spills using various detection systems that provide large-scale evaluations. The identification of an oil spill, utilizing SAR images is investigated in this study based on image analysis. Identification of the oil spill using change detection determines the changes over the images of the same location acquired at different times. In the proposed method, neighborhood based ratio feature is fed into Artificial neural network. The Difference Image (DI) generated by Neighborhood Ratio (NR) operator indicates local similarity between two images. Hierarchical Fuzzy c-means clustering approach is employed to separate interesting pixels with a greater possibility of having been modified or unmodified, and pseudo labels namely changed, unchanged, and intermediate class are assigned for the pixels. Pixel wise Neighborhood features are extracted based on image patches centered at the pixels of interest. Artificial Neural Network is trained to learn the model by employing these features. The trained neural network is used to classify intermediate class pixels. Finally the pre-classification and neural network classification results are combined to generate the final change map. The proposed methodology performs well for different datasets with accuracy above 90%.*

Index Terms - *Artificial Neural Network, Change Detection, Features, Oil Spill, SAR Image.*

INTRODUCTION

Oil spills in the ocean is one of the hazardous threats to deep ocean life with coastal eco system also being affected at multiple levels. Oil is obstinate and degrades in a very slow manner, hence, spilled oil makes multiple-layers over the surface of the ocean and remains for an intensive amount of time. Oil spills may be detected by remote sensing techniques which helps sensing the vast ocean through largely available satellite based data. Synthetic Aperture Radar (SAR) is an imaging system with high resolution. It is helpful and robust especially when the climate and light conditions are unfavorable. SAR works even in presence of dark clouds, dense fog and absence of sunlight. In recent days high resolution SAR satellite data are accessible like Radarsat-2, Terra-SAR and Cosmo/ Sky-Med that further enhance the wide range of applications. In this paper we use the SAR images for detection of the oil spills in ocean. SAR is microwave radar that is employed to form the 2 dimensional or 3 dimensional pictures of objects, oceans and landscapes. The resolution of SAR images is high and provides precise data. Change detection compares images of same location and different time stamps and is used in earth environment observation, Security and Risk Management.

Oil spill detection by Saima Naz et al. [1] involved Image Pre Processing -Image sub setting, Calibration, Speckle filtering, Multi-looking, Ellipsoid Correction, Land/Sea Marking. Dark Area Detection. Parameter Extraction and Image Classification. Xijun Liang et al. performed [2] Oil Spillage Identification using Ramp OC, in which Ramp Loss Function is employed and Kernel Based CCCP algorithm is used to train a Classifier. C. Bayındır et al. used Correlation coefficient change statistic and intensity ratio change statistic, to detect the oil spill and Double change map method is utilized to reduce the probability of false alarm. After an initial change map is created by adding time series images in a

 https://doi.org/10.37896/pd92.6/9268

ISSN: 0369-8963

way that excludes typical change areas while allowing uncommon change areas to be included, the first and last image in the temporal sequence are compared to produce a final change map [3]. Dongmei Song et al. [4] performed comparison and analysis of fully Pol-SAR features to identify the features which are suitable for Oil spillage identification. Image tonal contrast which is used to estimate the contrast of images, is used and the distances between peak values for the water surfaces and oil spills is utilized to select threshold and accurate identification of the oceanic oil Spillages from background sea water is performed using improved ACM(Active Contour Model) . Mishra, R. Balaji et al [5] implemented a Simple Approach for Oil Spill Detection combining Sentinel Application Platform (SNAP)-Ocean Application Tools and Texture Analysis .Pre- processing includes multi look, speckle filtering, radiometric calibration, ellipsoid correction. Peng Lie et al., [6] employed co-channel interference cancellation for denoising, and adaptive thresholding on GLCM features for oil spill detection. SAR images are denoised by Convolutional filters through detection of co-channel interference. GLCM texture analysis is used for oil spill identification. Four independent GLCM textural features namely energy, entropy, contrast and correlation are used. Adaptive thresholding is performed based on, window of 64 by 64 pixels around the current pixel If the grey value of current pixel was 15% less than the average, the current pixel was determined as oil spill, which would be otherwise taken as water. D Chaudhuri et al. [7] performed statistical image enhancement to boost the dark curvilinear features of the oil spill. Then, the curvilinear features are segmented using an iterative approach. The image is scanned for holes and filled and Graph theory is employed for thinning and pruning of branches. Geometric method based linking is finally performed to find the final oil spill trajectory. Guannan Li et al [8]., proposed improved polarimetric feature which is a combination based on polarimetric scattering entropy H and the improved anisotropy A_{12}–$H\_A_{12,}$ to distinguish oil spill from background sea water.

Fangjie Yu et al [9] proposed an adaptive mechanism based on Otsu method, which applies region growing combined with both edge detection and threshold segmentation (RGEDOM) to extract oil spills. In [10] Parth Praveen Deokar et al. used Sobel Edge Detection and Canny Edge Detection followed by morphological processing, erosion and dilation. In Krishna, Dhrisya et al., [11] detected oil spill using Region growing based segmentation followed by Canny edge detection. In [12] A. Brahma Tejaswini et al. detected the oil spill using Region splitting with merging based segmentation followed by Canny edge detection. The convolutional neural network Alex Net model is employed by Xinzhe Wang et al., [13] to extract details of oil spill information from SAR images by utilizing its properties of local connection, shared weights, and image representation learning. Topouzelis, Konstantinos N [14] isolated the dark areas and extracted its statistical characteristics and then compared them with statistical bases to classify as oil or look-alike. Feng Gao et al. [15] proposed the Change detection from synthetic aperture radar images based on Neighborhood-based Ratio (NR) and Extreme Learning Machine (ELM). NR operator is utilized for obtaining some pixels that have high probability of being changed or unchanged. Then, new image patches centered at these pixels are generated, and ELM is employed to train a model by using these patches. Finally, pixels in both original SAR images are classified by the pretrained ELM model. The ELM classification result and the pre-classification result are combined to form the final change map.

Symbolic Artificial Intelligence with its hard coding rules is incapable of solving these complex problems resulting in the introduction of Deep Learning (DL) models such as Recurrent Neural Networks and Convolutional Neural Networks (CNN). However, CNNs require lots of training data and are incapable of recognizing pose and deformation of objects leading to the introduction of Capsule Networks. Capsule Networks are the new sensation in Deep Learning. They have lived to this expectation as their performance in relation to the above problems has been better than Convolutional Neural Networks. Even with this promise in performance, lack of architectural knowledge and inner

 https://doi.org/10.37896/pd92.6/9268

ISSN: 0369-8963

workings of Capsules serves as a hindrance for researchers to take full advantage of this breakthrough Shaona Wang et al [16] proposed SAR image change detection based on sparse representation and a capsule network. Firstly, sparse features of the difference image (DI) are extracted by the Sparse Representation (SR) method. Secondly, a lightweight capsule network (L-Caps Net) is constructed, which is used to mine the spatial relationship between features. The network classifies the changed and unchanged pixels. Finally, the change map (CM) is generated. The proposed method can obtain more robust features while reducing the influence of speckle noise.

In this paper we propose oil spill identification based on the combination of change detection and Artificial Neural Network. For change detection Neighborhood Ratio (NR) operator is employed to generate difference image. Hierarchical Fuzzy c-means clustering approach is used to cluster the features and pseudo labels namely changed, unchanged and intermediate class are assigned to pixels. Artificial Neural Network is further employed to classify the intermediate class pixels with the training performed based on changed and unchanged class pixels.

MATERIALS AND METHODS

2.1 Change Detection

Wide range of images obtained by wide range of sensors such as radar, LiDAR, multispectral, or, optical, are frequently subjected to change detection (CD) mapping and analysis. Change detection algorithms analyses aircraft and satellite SAR imagery to identify changes caused by earthquakes, floods, tsunamis, storms, harsh snow and ice conditions, fires, and deforestation. Most of the mathematical approaches used for change detection have a tendency of extracting data about the changes that occur during a situation. The magnitude, location, and hence the direction of these changes are frequently within the scene's magnitude, location, and thus direction. In this paper we employ change detection to detect changes between the SAR images taken before the oil spill incident and after the incident.

2.2 Proposed Methodology

In this method Artificial Neural Network is employed along with Neighborhood Ratio(NR) computation, Hierarchical Fuzzy C-Means clustering (Hierarchical FCM) and Neighborhood feature extraction. The proposed methodology is explained in Figure 1. There are three primary steps in the proposed methodology:

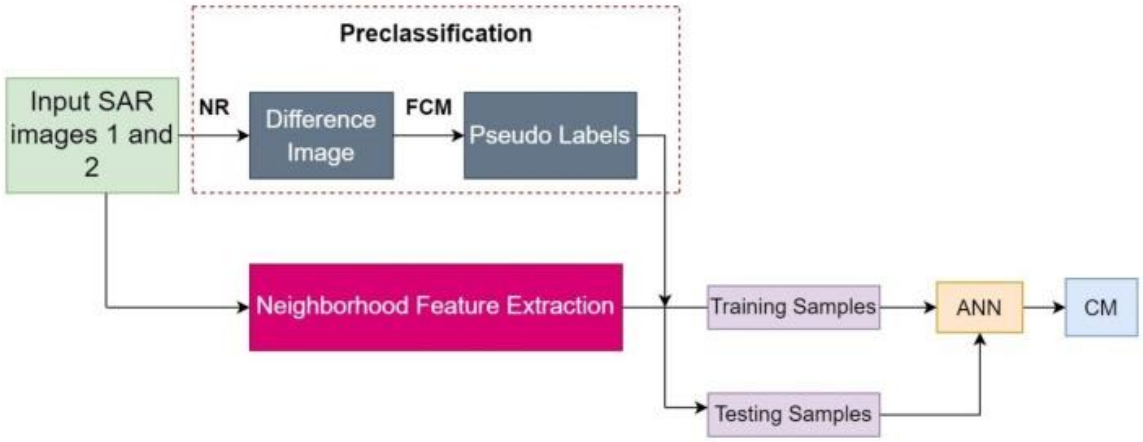

 https://doi.org/10.37896/pd92.6/9268

ISSN: 0369-8963

FIGURE I
FRAMEWORK OF THE PROPOSED CHANGE DETECTION METHOD

Step 1. Pre-classification using NR and FCM: Difference Image (DI) is computed by employing the NR operator. The Hierarchical FCM algorithm is then used to figure out the pixels that are most likely to change or remain unchanged. And these selected pixels are used to train ANN and the remaining pixels are categorized in step 3.

Step 2. Training a classifier by ANN: The patches centered on the pixels of interest selected in the previous step are used to train ANN. ANN is trained to classify as changed or unchanged based on pixel wise patch features

Step 3. Classification of intermediate pixels: The trained ANN based classifier is used to further divide the intermediate pixels from step 1 into changed and unchanged pixels. The final change map is then created by combining the ANN classification result and pre-classification result of step 1.

2.2.1 Data Used for Oil spill detection

Sentinal-1 SAR Images is employed for oil spill identification. The European Space Agency's SNAP sentinel application platform is a remote sensing toolbox architecture that provides tools for processing all common remote sensing satellite images. Copernicus Open Access Hub is used to download the data. The area of interest is selected from the world map displayed, with the satellite mission and the sensing period selection based on oil spill accident time and location, and the data is downloaded. After downloading the file from Copernicus open access hub, the product file is opened in SNAP software and the SAR image is extracted from VV band. And the required region is selected, and exported as image. SNAP software is used not only for extracting the data, but it also has many options to process the data like speckle noise removal, filtering etc.

2.2.2 Neighbourhood ratio

Neighbourhood ratio extraction is the first step in the proposed methodology. It employs the pixel by pixel operation on the input images. To construct a difference image, the neighborhood-based ratio (NR) operator is employed using the grey level information and spatial information of neighbor pixels. This operator can reduce the detrimental effects of speckle noise on SAR images. The difference image obtained, shows the local similarity between input SAR image 1 and input 2. NR operator is defined as follows

$$\mathrm{DI}(m,n) = \theta \times \frac{\min\{I_1(m,n), I_2(m,n)\}}{\max\{I_1(m,n), I_2(m,n)\}} + (1-\theta) \times \frac{\sum_{\in \Omega \wedge i \neq m,n} \min\{I_1(m,n), I_2(m,n)\}}{\sum_{\in \Omega \wedge i \neq m,n} max\{I_1(m,n), I_2(m,n)\}} \quad (1)$$

$$\theta = \frac{\sigma(m,n)}{\mu(m,n)} \quad (2)$$

The variance of the grey level in neighborhood $\mathrm{NR_{mn}}$ is represented by $\sigma(\mathrm{m},\mathrm{n})$. $\mathrm{NR_{mn}}$ has the size of r × r. Here we use r =5. The Gray level mean in the neighborhood $\mathrm{NR_{mn}}$ is represented by $\mu(\mathrm{m},\mathrm{n})$. $\mathrm{DI}(\mathrm{m},\mathrm{n})$ represents the intensity of a pixel in the generated DI at position (m,n). It provides the measure of the local similarity between input SAR image1 and input SAR image 2. The coefficient θ is the measure of local heterogeneity with small θ values indicating that the specified local region is homogeneous, while the large θ values suggesting that it is a varied local area or heterogeneous. The

 https://doi.org/10.37896/pd92.6/9268

ISSN: 0369-8963

Hierarchical FCM algorithm apply clustering to divide the pixels obtained in the Difference Image (DI) into three groups as the changed class Ω_c, unchanged class Ω_u, and intermediate class Ω_i.

Input: Difference Image (DI) generated by NR operator.
Step1: To partition pixels into two clusters Ω_c^1 and Ω_u^1, use the FCM algorithm on DI. T^1 represents the number of pixels in Ω_c^1. Then, $TT = \sigma.T^1$ is the threshold used to determine the upper bound of the change parameter. In our implementation, we've set σ at 1.20.
Step 2: To partition pixels into five clusters $\Omega_1^2, \Omega_2^2, \ldots, \Omega_5^2$, use the FCM algorithm on DI . The five clusters are listed in descending order by average values so that, the pixels in Ω_1^2 have the highest value, while pixels in Ω_5^2 have the lowest average value. Clusters with higher average value have a better chance of being in changed class. The size of the five clusters is referred as $T_1^2, T_2^2, \ldots, T_5^2$ respectively. Set the parameters to t = 1, and c= T_1^2. The pixels of Ω_1^2 is assigned as the class Ω_c.
Step 3: Set t = t+1, c = c+T_t^2.
Step 4: if c < TT, pixels of Ω_t^2 is assigned to the class Ω_i. Otherwise, pixels of Ω_t^2 is assigned to the class Ω_u. Return to step 3, and repeat until t = 5.
Output: The output of the pre-classification change map is represented as an image with labels {Ω_c, Ω_i, Ω_u}.

FIGURE II
HIERARCHICAL FCM CLUSTERING ALGORITHM

2.2.3 Hierarchical FCM clustering algorithm

Compared to FCM clustering, hierarchical FCM clustering can better segregate the pixels into changed and unchanged. The hierarchical FCM clustering algorithm is carried out in a series of steps that include input and output as given in Figure 2.

The pixels in Ω_c are more likely to have changed, while the pixels in Ω_u are more likely to have remained unchanged. These two types of pixels are used as training samples to train the ANN.

2.3.4 Neighborhood feature extraction and sample selections:

The neighborhood feature extraction is performed on selected patches from original image. Neighborhood features of SAR images are generated as follows:

New image patches (7x7) centered at each pixels are extracted directly from two original input SAR images. As seen in Figure 3. these image patches give sufficient change information around the region. Let $R_{mn}^{I_1}$ represent a patch in image I_1 with the centre at location (m, n) in I_1 with $R_{mn}^{I_1}$ being k × k in size. The equivalent patch in image I_2 is represented by $R_{mn}^{I_2}$. $R_{mn}^{I_1}$ and $R_{mn}^{I_2}$ are converted to vectors $V_{mn}^{I_2}$ and $V_{mn}^{I_2}$ respectively. These both vectors are combined to create a new vector V_{mn}. V_{mn}

 https://doi.org/10.37896/pd92.6/9268

ISSN: 0369-8963

represents the sample feature vector at the location (m, n). The training samples for the Artificial Neural Network are drawn from the sample feature vectors.

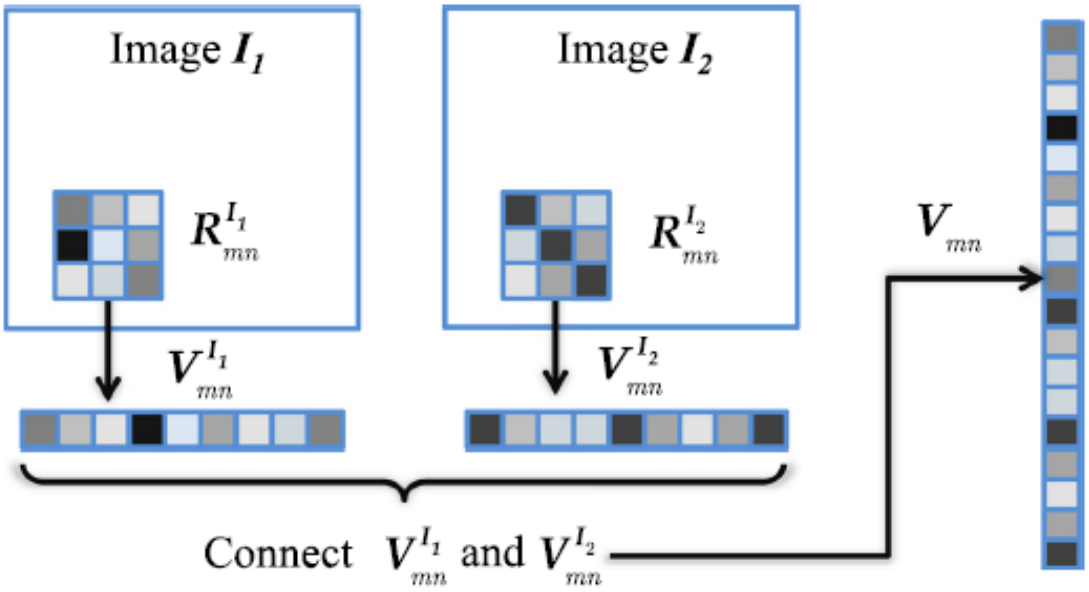

FIGURE III

NEIGHBORHOOD FEATURE GENERATION FOR EACH INTERESTED POSITION

The Neighborhood features of the selected pixels which belong to changed and unchanged class of pre-classification, are used to train the artificial neural network, with the labels of 0 and 1.

2.3.5 Artificial Neural Network (ANN):

Artificial neural networks (ANNs) are artificial brains that depict biological neural networks of the human brain. Connected units in ANN resemble the neurons in a biological brain. Three layers make up a neural network: input layer, hidden layer, and output layer. A layer is made up of small units known as neurons. The features are given as input to the neural network. A hidden layer is placed between the algorithm's input and output layer in neural networks, and it assigns weights to the inputs and guides them through an activation function to the output layer which is known as Feed forward propagation. In other words, the hidden layers conduct nonlinear modifications on the network's inputs. Then the output layer equates the output layer value to the labeled class value. The Back propagation fine-tunes mathematical weight functions and improves the accuracy of an artificial neural network's outputs. The error is calculated in the output layer based on the difference between the output value and the labeled value. Then the error along with the layers weight goes back to the previous layers to alter its weight and bias to get accurate output. The feed forward and back propagation repeats until the output has minimal error and good accuracy of output. The output of each neuron is calculated by the formula, Output = Sum (weights*inputs) + bias. The ANN learning algorithm is provided in Figure 5.

https://doi.org/10.37896/pd92.6/9268

ISSN: 0369-8963

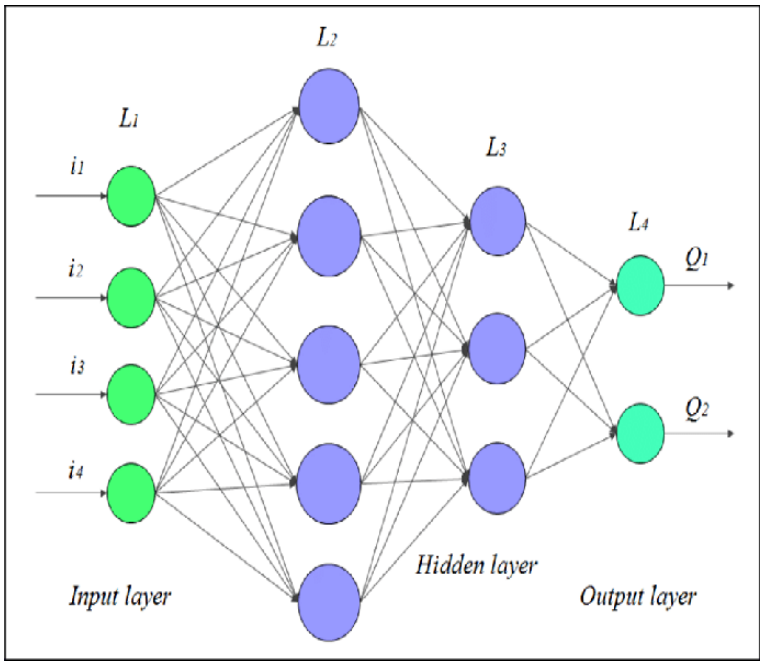

FIGURE IV

STRUCTURE OF ARTIFICIAL NEURAL NETWORK

Input: Pixels of interest selected by Hierarchial FCM, learning rate, Network .
Output: A trained Network
Step1: Assign the weights for input, hidden and output layers
Step 2: For I = 1 to numEpochs
For J = 1 to numTrainingdata
Do Forward Propagation
Compute Loss function
Do Back Propagation
Update Weights
Step 3 return the trained Network

FIGURE V

ANN LEARNING ALGORITHM

The parameters of Artificial Neural Network is selected as follows:

Maximum Iteration: 500
No. of Labels : 2 (0 and 1)
Hidden Layer : square root (no. of label* input neuron)
Activation Function: Sigmoid $S(x) = \frac{1}{1+e^{-x}}$

https://doi.org/10.37896/pd92.6/9268

ISSN: 0369-8963

Validation percentage: 20

The Training samples are trained and validated in neural network. The testing samples, the neighborhood features of pixels corresponding to Ω_i are given as input into the trained ANN, and the intermediate pixels are classified into the changed and unchanged classes. The final change map is then created by merging the pre-classification result and Artificial neural network classification result.

EXPERIMENTAL SETUP

The implementation of the proposed work is done using Matlab 2020a in a personal computer having Intel (R) core i5 and 64-bit processor with 8 GB RAM. The datasets used for the performance evaluation include the Chennai Oil spill data, the San Francisco dataset, the Bern dataset, the Ottawa dataset the Farmland dataset and the Yellow River dataset. The performance measures namely Kappa Coefficient (KC) and Percentage Correct Classification (PCC) are used to evaluate the performance of the proposed methodology.

RESULTS AND DISCUSSION

The Chennai Oil spill data is acquired by sentinel-1 through Copernicus open hub and format converted through SNAP tool. The images were captured in January 2016 (Figure 6(a)) and January 2017 (Figure 6(b)). These images are given as input to the algorithm. The Final change map obtained by proposed method is shown in Figure 6(c)

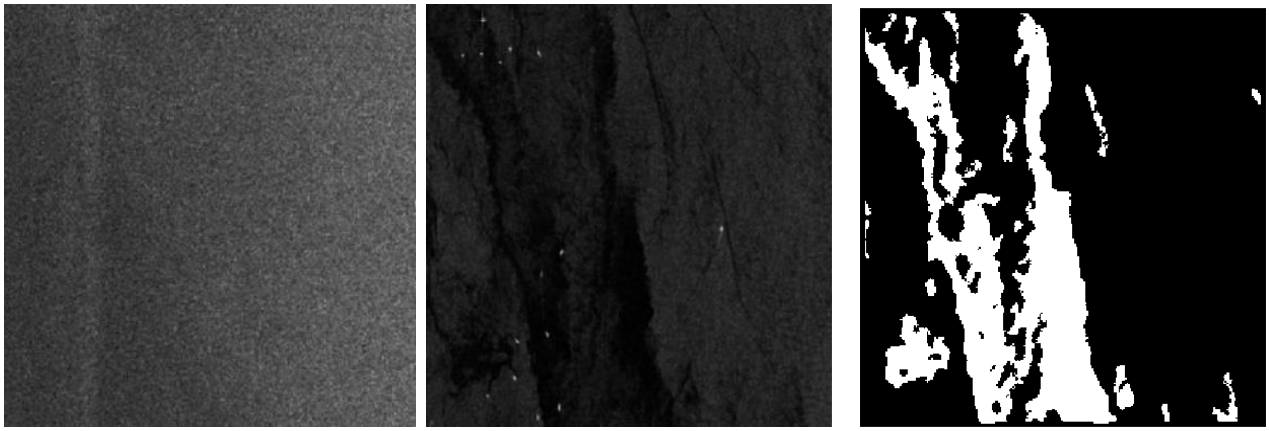

(a) (b) (c)

Figure VI
CHENNAI OIL SPILL DATA. (A) IMAGE ACQUIRED IN 2016 (B) IMAGE ACQUIRED IN 2017 (C) OIL SPILL DETECTED OUTPUT

https://doi.org/10.37896/pd92.6/9268

ISSN: 0369-8963

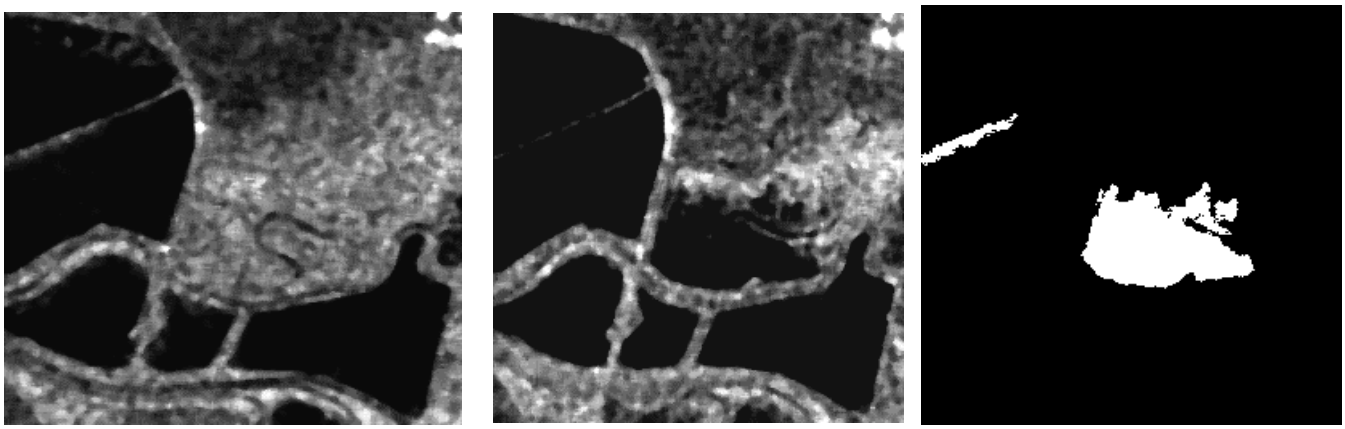

‘ (a) (b) (c)

FIGURE VII
(A) SAN FRANCISCO DATASET ACQUIRED IN AUGUST 2003 (B) SAN FRANCISCO DATASET ACQUIRED IN MAY 2004. (C) GROUND-TRUTH IMAGE

The quantitative measures used to evaluate the performance of the proposed method include False Positives (FP), False Negatives (FN), Overall Error (OE), and Percentage Correct Classification (PCC). We test the proposed method on five more SAR datasets, each with its own set of characteristics.

The San Francisco dataset is the first one, as seen in Figure 7. It shows a part of two SAR images captured by the ERS-2 SAR sensor (256x256 pixels). The images were taken in August of 2003 and May of 2004. The ground truth change map in Figure 7(c) is ground truth created by combining prior knowledge with human interpretation of Figures 7(a) and 7(b).

The Bern dataset was the second dataset utilized in this experiment. It's made up of two SAR images taken by the ERS-2 satellite in April and May of 1999, By combining prior knowledge with human interpretation, the generated ground truth is given in Figure. 8(c).

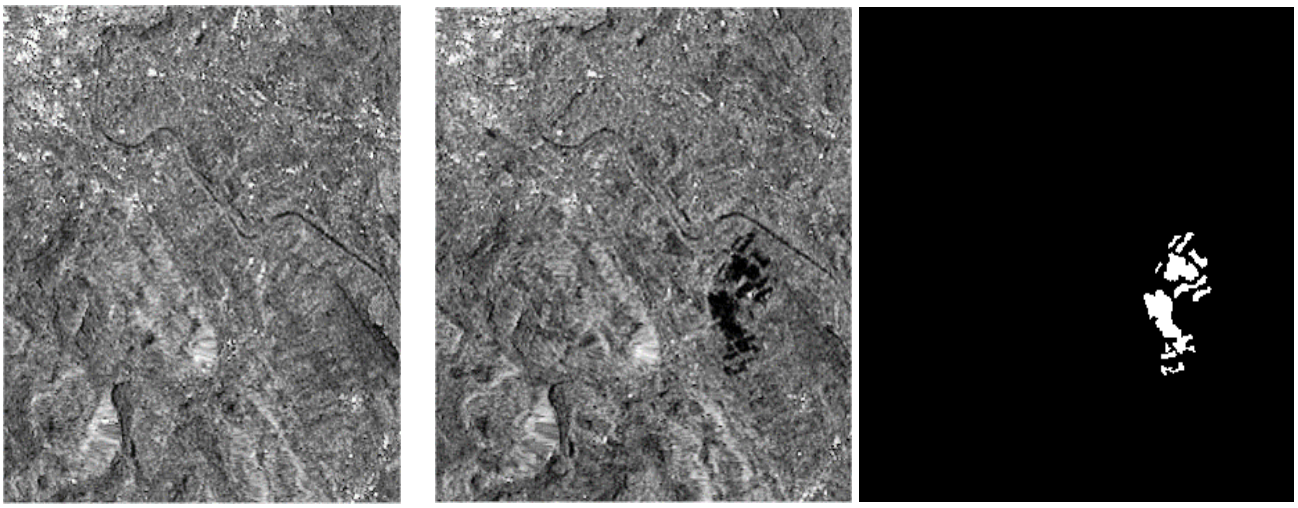

(a) (b) (c)

FIGURE VIII
(A) BERN DATASET ACQUIRED IN JUNE 2008. (B) BERN DATASET ACQUIRED IN JUNE 2009. (C) GROUND-TRUTH IMAGE.

 https://doi.org/10.37896/pd92.6/9268

ISSN: 0369-8963

The Ottawa dataset was the third dataset used for the experimentation. It is a segment (290 x 350 pixels) of two SAR images obtained by the RADARSAT SAR sensor above the city of Ottawa. It contains two images, one from May 1997 and the other from August 1997. The images depict locations that have changed after they were flooded. The ground truth Figure 9(c) was developed by combining previous data with photo interpretation.

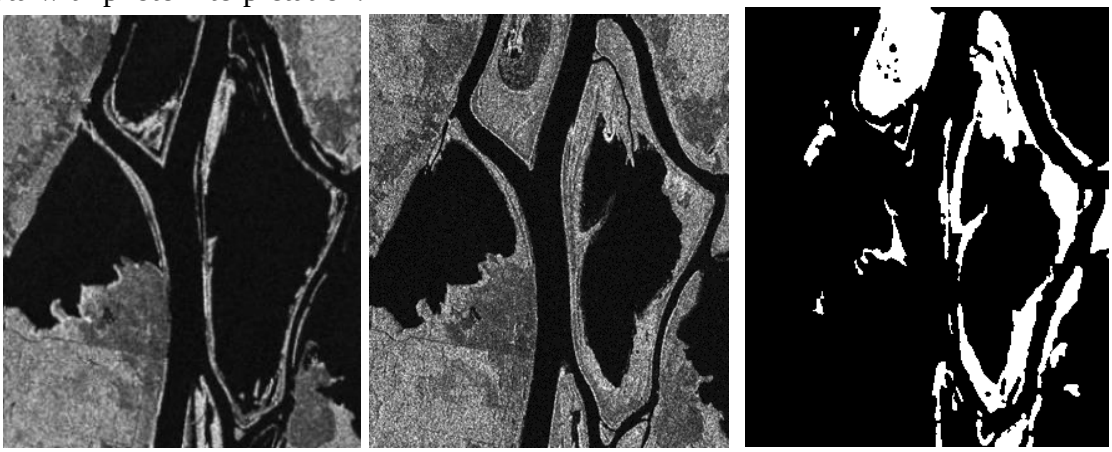

(a) (b) (c)

FIGURE IX
(A) OTTAWA DATASET ACQUIRED IN MAY 1997. (B) OTTAWA DATASET ACQUIRED IN AUGUST 1997. (C) GROUND-TRUTH IMAGE

https://doi.org/10.37896/pd92.6/9268

ISSN: 0369-8963

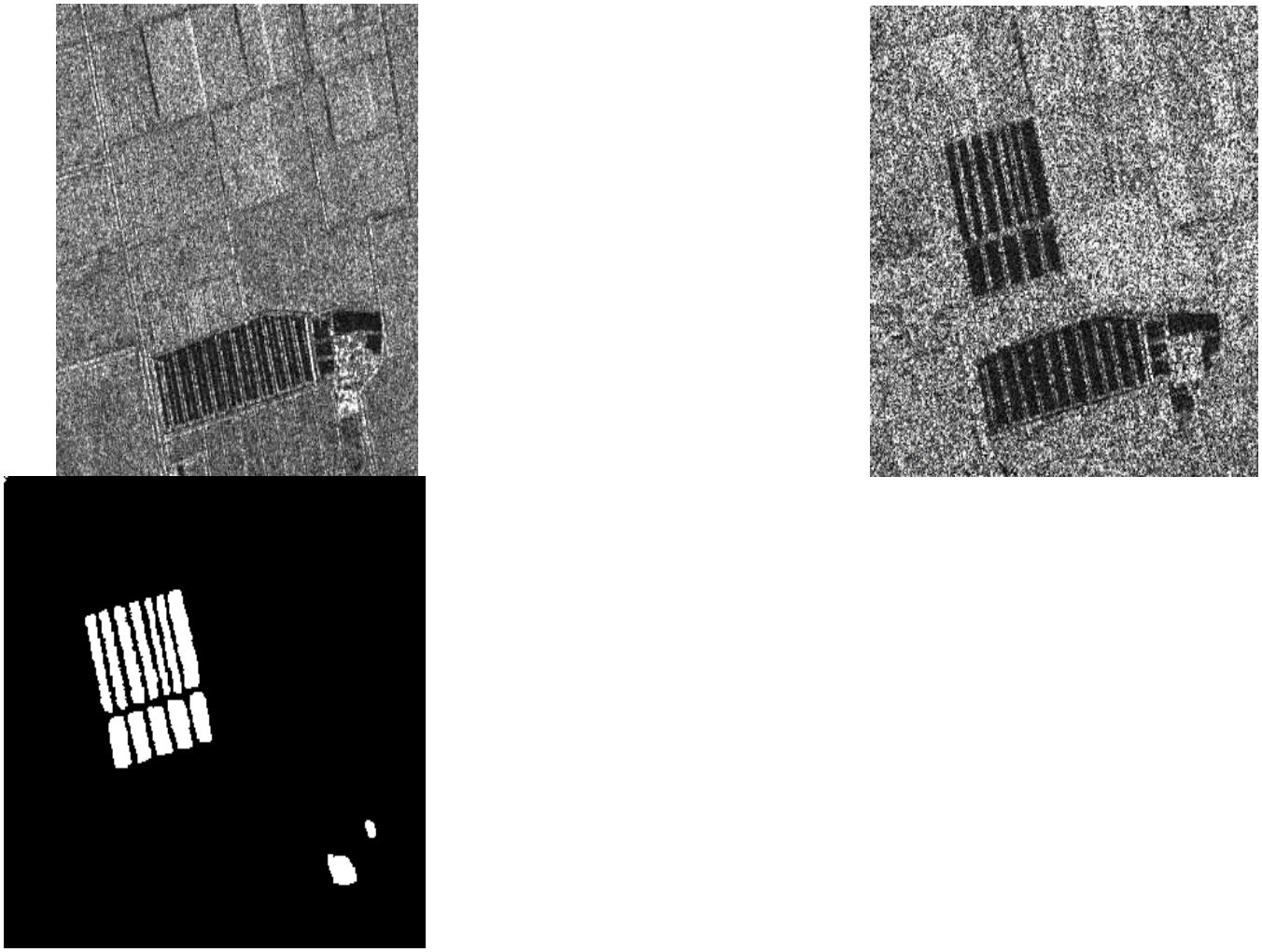

(a) (b) (c)

FIGURE X
(A) FARMLAND DATASET ACQUIRED IN JUNE 2008. (B) FARMLAND DATASET ACQUIRED IN JUNE 2009. (C) GROUND-TRUTH IMAGE

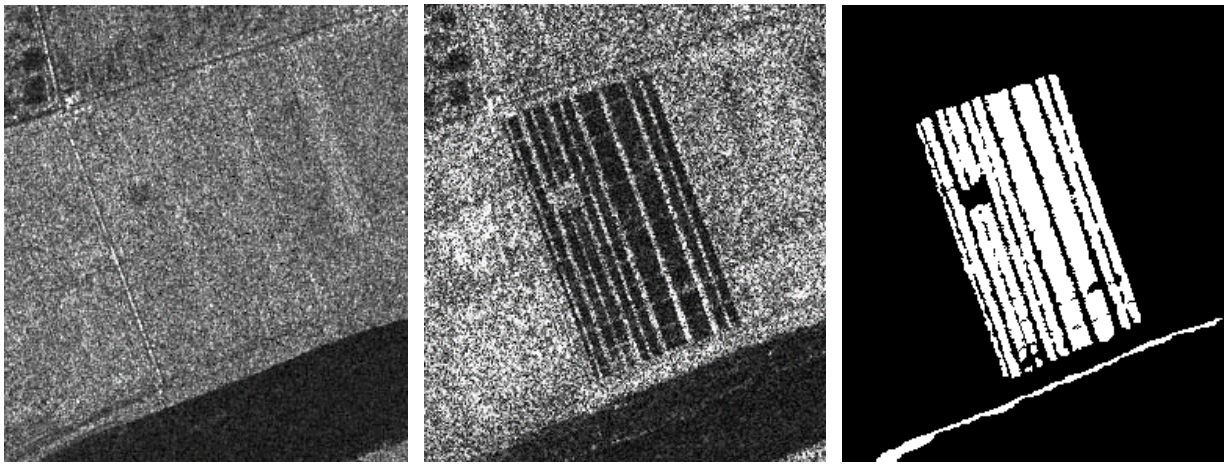

(a) (b) (c)

https://doi.org/10.37896/pd92.6/9268

ISSN: 0369-8963

FIGURE XI
(A) YELLOW RIVER DATASET ACQUIRED IN JUNE 2008. (B) YELLOW RIVER DATASET ACQUIRED IN JUNE 2009. (C) GROUND-TRUTH IMAGE

The fourth and fifth dataset namely the Farmland dataset and the Yellow River dataset, has Radarsat-2 SAR images of the Yellow River Estuary in China taken between June 2008 and June 2009.

Due to the vast size of the Yellow River dataset, we chose two sample regions: Farmland and Yellow River. The images are 306x291 and 257x287 pixels in size. Ground truth was established by combining prior information with photo interpretation, as seen in Figures 10(c) and 11(c).

3.1 Test of the Parameter 'r'

The first experiment is a test of the NR operator's parameter r, which refers to the size of the neighborhood. It was chosen as the test parameter because it is linked to pre-classification accuracy.

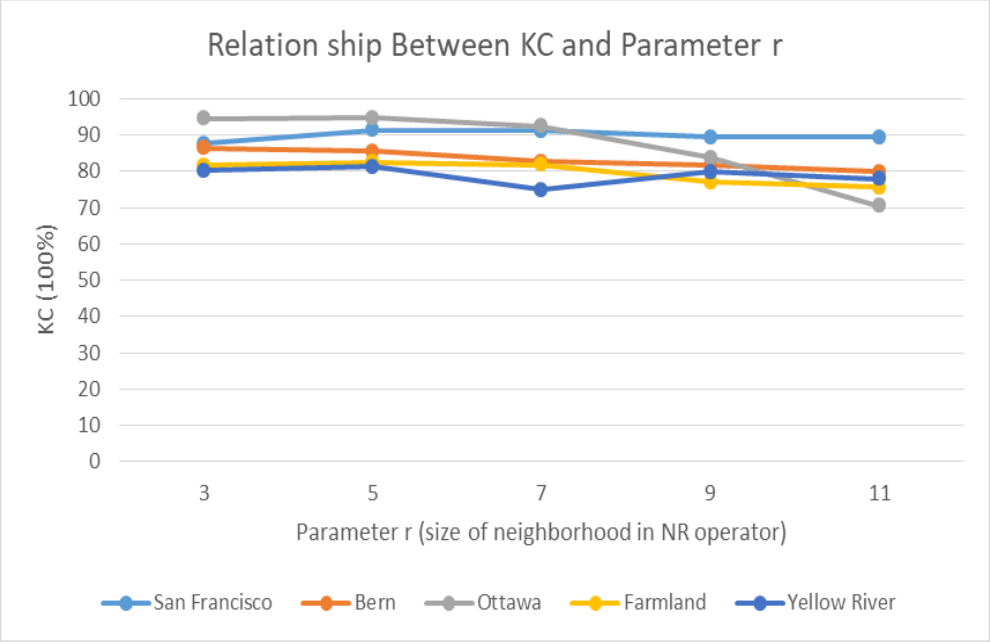

FIGURE XII
PERFORMANCE MEASURE (KC) FOR DIFFERENT NEIGHBOURHOOD SIZE OF THE NR OPERATOR ON OTHER SAR DATASETS

In this experiment, r has discrete values and ranges from 3 to 11. The SAR datasets are used in this experiment, and the purposeful criterion KC is used. Figure 11 depicts the results. The five curves show how the values of KC change as the size of r increases. It is maximum at value 5. As a result, in the following trials, we set the NR operator's neighborhood size to 5 × 5.

3.2 Test of the Parameter 'k'

The second experiment is a test of the feature extraction parameter k, which stands for neighborhood size. The size of the neighborhood is a critical factor that can influence the final outcomes of change detection.

https://doi.org/10.37896/pd92.6/9268

ISSN: 0369-8963

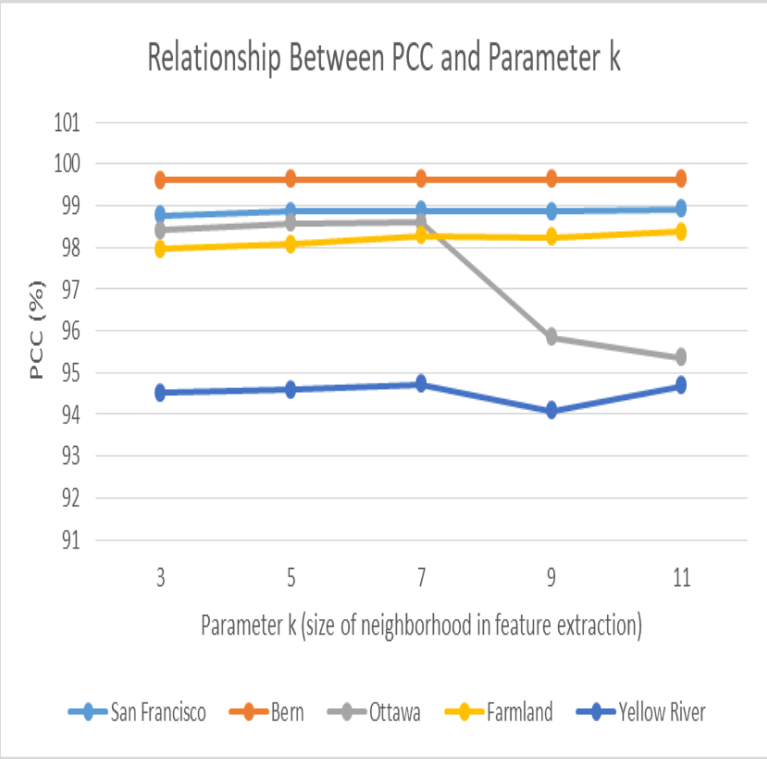

FIGURE XIII
PERFORMANCE MEASURE (PCC) FOR DIFFERENT FEATURE EXTRACTION PARAMETER 'K' ON OTHER SAR DATASETS

PCC is used as the criterion here, and the five SAR datasets are tested. We set k to 3, 5, 7, 9, and 11 to show the link between k and PCC, as shown in Figure 13. The ANN classifier requires a large enough neighborhood patch for feature learning; the five curves show how the values of KC change as 'k' grows larger. By observing the PCC on differing the k, on the majority of datasets, the proposed technique performs best when k is set to 7. As a result, the optimal k value for feature extraction is k = 7. For feature extraction with Artificial Neural Network, we utilize a neighbourhood of 7 pixels in the following tests.

3.3 Results of other Datasets

These 5 datasets are used to analyze effectiveness of our method. The images from these datasets are given as input to the proposed method and their change maps are generated as shown in Figure 14. The actual number of pixels in the binary ground truth image that belong to the unmodified and changed classes are counted (denoted by N_u and N_c, respectively). On the other hand, the binary ground truth image is compared with the created change map pixel by pixel using a specific algorithm. The number of pixels that belong to the unchanged class but are incorrectly labelled as changed class is then denoted by False Positives FPs. The amount of pixels that correspond to the changed class but are incorrectly labelled as unchanged class is referred to as False Negatives FNs. The total error (OEs) is the sum of the FP and FN errors.

https://doi.org/10.37896/pd92.6/9268

ISSN: 0369-8963

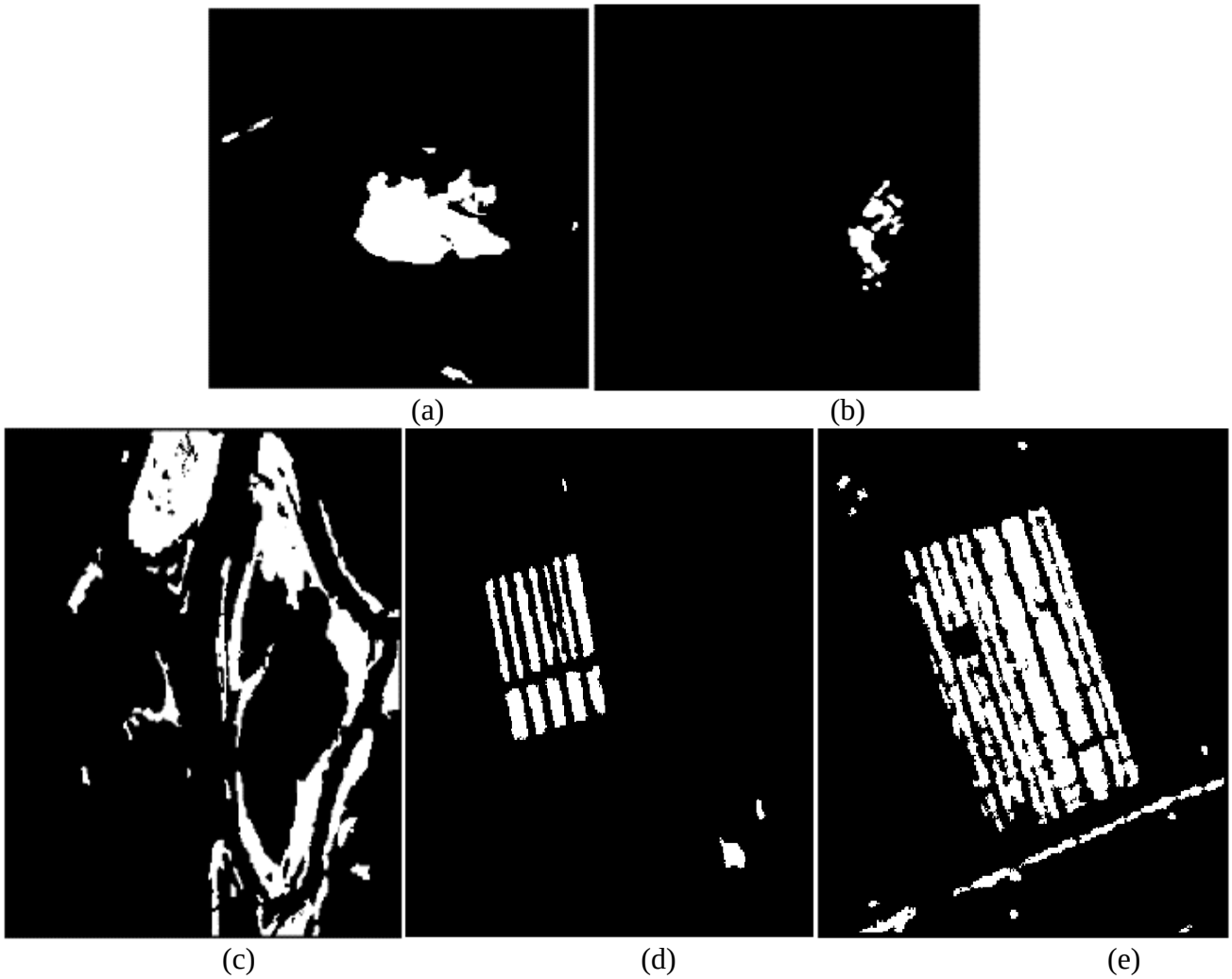

(a) (b)

(c) (d) (e)

FIGURE XIV

FINAL CHANGE MAP OF (A) SAN DATASET. (B) BERN DATASET. (C) OTTAWA DATASET. (D) FARMLAND DATASET. (E) YELLOW RIVER DATASET BY PROPOSED METHOD

Percentage Correct Classification (PCC) is given by

$$PCC = \frac{N_u + N_c + FP + FN}{N_c \ X \ N_u} \ X \ \ 100\% \qquad (3)$$

KC calculates the percentage of agreement (correctly classified pixels) after adjusting for the amount of agreements that would be predicted by chance. Specifically, KC is defined as

$$KC = \frac{PCC - PE}{1 - PE} \qquad (4)$$

Where,

$$PE = \frac{(N_c - FN + FP)N_c + (N_u - FP + FN)N_u}{(N_c + N_u)(N_c + N_u)} \qquad (5)$$

It's worth mentioning that KC is based on the dependent values of FP and FN, whereas PCC is based only on the total of FP and FN. Because when more comprehensive information is involved, KC is a more convincing coefficient than PCC.

The other SAR data is given to proposed method and its efficiency is evaluated by quantity measures FN, FP, OE, PCC and KC and they are tabulated in Table 1.

 https://doi.org/10.37896/pd92.6/9268

ISSN: 0369-8963

TABLE I
CHANGE DETECTION RESULT OF PROPOSED METHOD ON THE DIFFERENT DATASET

DATA	FN	FP	OE	PCC (%)	KC (%)
San Francisco	434	303	737	98.88	91.42
Bern	186	139	325	99.64	85.46
Ottawa	788	633	1421	98.60	94.72
Farmland	1464	63	1527	98.29	82.41
Yellow River	2932	945	3877	94.78	82.41

3.4 Comparison with conventional methods:

The Comparison of the proposed method with the conventional methods is provided in the Table 2. The proposed method has better accuracy with reduced computational complexity.

TABLE II
COMPARISON OF THE PERFORMANCE OF THE PROPOSED METHOD WITH CONVENTIONAL METHODS

DATA	PCC (%)
Fuzzy Classification (Nirchio et al.)[17]	90
Probabilistic Approach (Solberg et al.)[18]	97.08
ANN + (Color, Shape features)(Topouzelis et al.)[19]	91
CNN (Kan Zeng et al)[20]	78
Proposed Method	98.04

CONCLUSION

In this paper, an efficient methodology for Oil Spill detection in the Ocean using SAR Images is presented employing Change Detection. Neighborhood Ratio of the image is utilized to create a difference image and Hierarchical FCM is employed to cluster and assign pseudo labels for changed, unchanged and intermediate pixels. ANN is trained and tested with neighborhood features of changed and unchanged pixels to classify the intermediate pixels into changed and unchanged class. Final Change Map is obtained for two SAR images by combining the result of pre-classification and Artificial Neural Network classification. Despite taking into account the degree of the NRCS reduction relative to the background, the position/shape of the dark area, and the texture of the dark feature, it also takes into account the change before and after the accident. The proposed method gives good performance for wide range of datasets and the performance is validated with the help of Percentage Correct Classification. And Kappa Co-efficient.

ACKNOWLEDGMENT

We are grateful to the principal and the management of Mepco Schlenk Engineering College for providing outstanding support.

 https://doi.org/10.37896/pd92.6/9268

ISSN: 0369-8963

REFERENCES

[1] Saima Naz, Muhammad Farooq Iqbal, Irfan Mahmood, Mona Allam. Marine oil spill detection using Synthetic Aperture Radar over Indian Ocean", Elseveir, Marine Pollution Bulletin, Volume 162, January 2021, 111921 December, 2020.

[2] Xijun Liang, Zongjin Zhen, Yunquan Song, Ling Jian and Dongmei Song, Pol-SAR Based Oil Spillage Classification with Various Scenarios of prior Knowledge, IEEE Journal of Ocean Engineering, Vol.43, No. 1, May, 2019.

[3] C. Bayındır, J. D. Frost and C. F. Barnes, "Assessment and Enhancement of SAR Noncoherent Change Detection of Sea-Surface Oil Spills," in *IEEE Journal of Oceanic Engineering*, vol. 43, no. 1, pp. 211-220, Jan. 2018, doi: 10.1109/JOE.2017.2714818.

[4] D. Song *et al*., "An Efficient Marine Oil Spillage Identification Scheme Based on an Improved Active Contour Model Using Fully Polarimetric SAR Imagery," in *IEEE Access*, vol. 6, pp. 67959-67981, 2018, doi: 10.1109/ACCESS.2018.2876173.

[5] Mishra, A., Balaji, R. Simple Approaches to Oil Spill Detection Using Sentinel Application Platform (SNAP)-Ocean Application Tools and Texture Analysis: A Comparative Study. J Indian Soc Remote Sens 45, 1065-1075 ,2017.

[6] Peng Liu, Ying Li, Jin Xu & Tong Wang , Oil spill extraction by X-band marine radar using Texture analysis and adaptive thresholding, Remote Sensing Letters,10:6, 583-589, 2019.

[7] D. Chaudhuri et al., "A Statistical Approach for Automatic Detection of Ocean Disturbance Features from SAR Images," in IEEE Journal of Selected Topics in Applied Earth Observations and Remote Sensing, vol. 5, no. 4, pp. 1231-1242, Aug. 2012, doi: 10.1109/JSTARS.2012.2186630.

[8] Li, Guannan, Ying Li, Yongchao Hou, Xiang Wang, and Lin Wang. "Marine Oil Slick Detection Using Improved Polarimetric Feature Parameters Based on Polarimetric Synthetic Aperture Radar Data" Remote Sensing 13, no. 9: 1607, 2021.

[9] Fangjie Yu, Wuzi Sun, Jiaojiao Li, Yang Zhao, Yanmin Zhang, Ge Chen, An improved Otsu method for oil spill detection from SAR images, Oceanologia, Volume 59, Issue 3,2017,

[10] Parth Praveen Deokar, Shaswata Rout, Debarati Datta, S. Sivapriya, Oil Spill and Debris Detection using Image, International Journal of Engineering and Advanced Technology (IJEAT) ISSN: 2249-8958, Volume-8 Issue-5, June 2019.

[11] Krishna, Dhrisya & Keerthi. Oil Spill Detection from Synthetic Aperture Radar Image through Improved Edge Detection Method. International Journal of Computer Sciences and Engineering. 6. 500-505, 2018.

[12] A. Brahma Tejaswini, Dr. P. Siddaiah, 2021, Implementation of Oil Spill Detection from SAR Image through Improved Canny Edge Detection, International Journal Of Engineering Research & Technology (IJERT) vol. 10, no. 03 March 2021.

[13] Xinzhe Wang, Jiaxu Liu, Shuai Zhang, Qiwen Deng, Zhuo Wang, Yunhao Li,and Jianchao Fan, Detection of Oil Spill Using SAR Imagery Based on AlexNet Model, Hindawi Computational Intelligence and Neuroscience ,2021,

[14] Topouzelis, Konstantinos N.. "Oil Spill Detection by SAR Images: Dark Formation Detection, Feature Extraction and Classification Algorithms" *Sensors* 8, no. 10: 6642-6659, 2008.

[15] Feng Gao, Junyu Dong, Bo Li, Qizhi Xu, Cui Xie, "Change detection from synthetic aperture radar images based on neighborhood-based ratio and extreme learning machine," J. Appl. Remote Sens. 10(4), 046019 ,2016.

 https://doi.org/10.37896/pd92.6/9268

ISSN: 0369-8963
[16] Shaona Wang, Yanan Wang, Yang Liu & Linlin Li SAR image change detection based on sparse representation and a capsule network, Remote Sensing Letters, 12:9, 890-899, 2021

[17] Nirchio, F.; Sorgente, M.; Giancaspro, A.; Biamino, W.; Parisato, E.; Ravera R.; Trivero, P. Automatic detection of oil spills from SAR images. Int. J. Remote Sens. 2005, 26 (6), 1157–1174.

[18] Solberg, A.; Brekke, C.; Husoy P.O. Oil spill detection in Radarsat and Envisat SAR images. IEEE Trans. Geosci. Remote Sens. 2007, 45, 746-755.

[19] Topouzelis, K.; Stathakis, D.; Karathanassi, V. Investigation of genetic algorithms contribution to feature selection for oil spill detection. Int. J. Remote Sens. 2008

Kan Zeng; Yixiao Wang. A Deep Convolutional Neural Network for Oil Spill Detection from Spaceborne SAR Images. Int. J. Remote Sens. 2020

 https://doi.org/10.37896/pd92.6/9268